Highly-efficient fully resonant vertical couplers for InP active-passive monolithic integration using vertically phase matched waveguides

Óscar García López,[1,2,*] Daniel Lasaosa,[1] Manuel López-Amo,[1] and Marko Galarza[1]

[1]*Department of Electric and Electronic Engineering, Universidad Pública de Navarra,Campus Arrosadia s/n, 31006 Pamplona, Spain*

[2]*Fundación Cetena, 31110 Noain, Spain*

[*]*ogarcia@cemitec.com*

Abstract: A new active-passive monolithic integration approach for photonic components based on vertical evanescent coupling is presented. Two vertically stacked waveguides are used in order to provide full resonant power transfer between them and avoiding the need of tapered structures. Light confinement in each waveguide is achieved combining strong lateral asymmetric structures and bent waveguides, both defined during lithography. Low propagation losses for the active waveguide and coupling efficiencies to the passive section as high as 97% have been obtained.

OCIS codes: (130.0130) Integrated optics; (130.3120) Integrated optics devices.

References and links

1. J. D. Meindl, Q. Chen, and J. A. Davis, "Limits on silicon nanoelectronics for terascale integration," Science **293**(5537), 2044–2049 (2001).
2. M. Lundstrom, "Applied physics. Moore's law forever?" Science **299**(5604), 210–211 (2003).
3. D. J. Blumenthal, J. Barton, N. Beheshti, J. E. Bowers, E. Burmeister, L. A. Coldren, M. Dummer, G. Epps, A. Fang, Y. Ganjali, J. Garcia, B. Koch, V. Lal, E. Lively, J. Mack, M. Mašanović, N. McKeown, K. Nguyen, S. C. Nicholes, Hyundai Park, B. Stamenic, A. Tauke-Pedretti, H. Poulsen, and M. Sysak, "Integrated photonics for low-power packet networking," IEEE J. Sel. Top. Quantum Electron. **17**(2), 458–471 (2011).
4. D. Liang and J. E. Bowers, "Photonic integration: Si or InP substrates?" Electron. Lett. **45**(12), 578–581 (2009).
5. C. Cole, B. Huebner, and J. E. Johnson, "Photonic integration for high-volume, low-cost applications," IEEE Commun. Mag. **47**(3), S16–S22 (2009).
6. R. Nagarajan, C. H. Joyner, R. P. Schneider, Jr., J. S. Bostak, T. Butrie, A. G. Dentai, V. G. Dominic, P. W. Evans, M. Kato, M. Kauffman, D. J. H. Lambert, S. K. Mathis, A. Mathur, R. H. Miles, M. L. Mitchell, M. J. Missey, S. Murthy, A. C. Nilsson, F. H. Peters, S. C. Pennypacker, J. L. Pleumeekers, R. A. Salvatore, R. K. Schlenker, R. B. Taylor, Huan-Shang Tsai, M. F. Van Leeuwen, J. Webjorn, M. Ziari, D. Perkins, J. Singh, S. G. Grubb, M. S. Reffle, D. G. Mehuys, F. A. Kish, and D. F. Welch, "Large-scale photonic integrated circuits," IEEE J. Sel. Top. Quantum Electron. **11**(1), 50–65 (2005).
7. G. Grasso, P. Galli, M. Romagnoli, E. Iannone, and A. Bogoni, "Role of integrated photonics technologies in the realization of terabit nodes [Invited]," J. Opt. Commun. Netw. **1**(3), B111–B119 (2009).
8. J. J. G. M. Van Der Tol, Y. S. Oei, U. Khalique, R. Ntzel, and M. K. Smit, "InP-based photonic circuits: Comparison of monolithic integration techniques," Prog. Quantum Electron. **34**(4), 135–172 (2010).
9. R. Nagarajan, M. Kato, J. Pleumeekers, P. Evans, S. Corzine, S. Hurtt, A. Dentai, S. Murthy, M. Missey, R. Muthiah, R. A. Salvatore, C. Joyner, R. Schneider, M. Ziari, F. Kish, and D. Welch, "InP photonic integrated circuits," IEEE J. Sel. Top. Quantum Electron. **16**(5), 1113–1125 (2010).
10. Y. Suematsu, M. Yamada, and K. Hayashi, "Integrated Twin-Guide AlGaAs laser with multiheterostructure," IEEE J Quantum Electron QE **11**(7), 457–460 (1975).
11. P. V. Studenkov, M. R. Gokhale, J. C. Dries, and S. R. Forrest, "Monolithic integration of a quantum-well laser and an optical amplifier using an asymmetric twin-waveguide structure," IEEE Photon. Technol. Lett. **10**(8), 1088–1090 (1998).
12. F. Xia, V. M. Menon, and S. R. Forrest, "Photonic integration using Asymmetric Twin-Waveguide (ATG) technology: Part I - Concepts and theory," IEEE J. Sel. Top. Quantum Electron. **11**(1), 17–29 (2005).
13. V. M. Menon, F. Xia, and S. R. Forrest, "Photonic integration using Asymmetric Twin-Waveguide (ATG) technology: Part II-devices," IEEE J. Sel. Top. Quantum Electron. **11**(1), 30–42 (2005).

#193754 - $15.00 USD Received 11 Jul 2013; revised 27 Aug 2013; accepted 27 Aug 2013; published 19 Sep 2013

14. M. Galarza, D. Van Thourhout, R. Baets, and M. Lopez-Amo, "Compact and highly-efficient polarization independent vertical resonant couplers for active-passive monolithic integration," Opt. Express **16**(12), 8350–8358 (2008).
15. X. Sun and A. Yariv, Supermode control in integrated hybrid Si/III-V optoelectronic circuits for modal gain enhancement" in CLEO/Pacific Rim 2009 - 8th Pacific Rim Conference on Lasers and Electro-OpticsAnonymous, 5292330, (2009).
16. A. Yariv, "Coupled-mode theory for guided-wave optics," IEEE J Quantum Electron QE **9**(9), 919–933 (1973).
17. J. Hu and C. R. Menyuk, "Understanding leaky modes: Slab waveguide revisited," Adv. Opt. Photonics **1**(1), 58–106 (2009).
18. A. S. Sudbo, "Numerically stable formulation of the transverse resonance method for vector mode-field calculations in dielectric waveguides," IEEE Photon. Technol. Lett. **5**(3), 342–344 (1993).
19. C. Vassallo and J. M. Van Der Keur, "Comparison of a few transparent boundary conditions for finite-difference optical mode-solvers," J. Lightwave Technol. **15**(2), 397–402 (1997).
20. J. E. Schramm, D. I. Babic, E. L. Hu, J. E. Bowers, and J. L. Merz, "Fabrication of high-aspect-ratio InP-based vertical-cavity laser mirrors using CH4/H2/O2/Ar reactive ion etching," J. Vac. Sci. Technol. B **15**(6), 2031–2036 (1997).
21. L. M. Augustin, J. J. G. M. van der Tol, R. Hanfoug, W. J. M. de Laat, M. J. E. van de Moosdijk, P. W. L. van Dijk, Y.-S. Oei, and M. K. Smit, "A single etch-step fabrication-tolerant polarization splitter," J. Lightwave Technol. **25**(3), 740–746 (2007).

1. Introduction

The explosive growth of the Internet due to consumer applications like video on demand (VOD) has increased remarkably the necessity of bandwidth from the communication networks. In order to cope with this need it is predicted that the capacity of those networks will grow exponentially in the next years. However, the electronic integrated circuits are reaching their physical integration limit [1–3] and Photonic Integrated Circuits (PIC) arise as the natural evolution of the formers owing to their higher bandwidth and lower power consumption. Nevertheless, finding a standardized photonic integration technology is not a trivial issue [4–7] in part due to the great difficulty to integrate the three basic photonic functions (guiding, amplification and detection) in the same host material. One of the most promising photonic integration technology is InP-based monolithic integration [8,9].

Over the past years several active-passive integration techniques have been developed. Butt-joint regrowth, selective area growth, quantum well intermixing and offset quantum wells are complex and expensive technologies that result in high cost devices and/or low yields. Suematsu, et al. [10] proposed the integrated twin-guide structure (TG) where the active and passive functions are separated into two different vertically displaced waveguides, eliminating the need for material regrowth or any post-growth processing. Due to the phase matching condition, efficient light power transfer is achieved between both waveguides; this matching however, is a drawback when keeping light in the active core in order to reach high gain since optical power is constantly going up and down due to the full resonant mode beating phenomenon between the odd and even modes of the structure. As a consequence, any device based on Suematsu's structure is strongly dependent of its length, resulting in the inability to control critical parameters like the lasing threshold current of a laser or the modal gain in a semiconductor optical amplifier. This integration concept is also known as vertical evanescent coupling.

Several years later, the authors in [11–13] proposed the use of asymmetric twin-waveguides (ATG) with taper couplers. They utilize an active waveguide with a higher effective index than the passive waveguide, making them strongly asymmetric. Under this condition the even mode dominates in the active devices due to its larger gain and the odd mode is never excited, allowing the independent optimization of the active devices. The power transfer to the passive waveguide is realized using adiabatic tapers implying rather long designs and sub-micron final taper tips (~0.5 μm), which are difficult to achieve by standard lithography. In a previous work we demonstrate an approach to solve these drawbacks in ATG waveguides [14].

In this paper a new concept for monolithic InP-based integration of active and passive optical devices based on vertically coupled phase matched waveguides is presented. The

#193754 - $15.00 USD Received 11 Jul 2013; revised 27 Aug 2013; accepted 27 Aug 2013; published 19 Sep 2013

proposed structure provides: 1) an optimum confinement of light in each waveguide when needed, and 2) the fully resonant coupling between the active and the passive waveguide over a considerably shorter length and without the need of sub-micron lithography.

2. Concept

Figure 1 shows a three dimensional representation of the integration technology proposed in this paper. The two vertically stacked phase matched quaternary cores are shown using the same gray color, whereas the InP substrate and claddings are filled white. In section A, the active waveguide is defined over the unetched passive waveguide. Such a structure drastically breaks the phase matching condition between both waveguides, allowing light to be confined in the active core. In section B, the stacked active and passive waveguides are defined with the same width creating a vertical directional coupler. The active mode reaching section B excites equally both supermodes providing resonant coupling of light to the underlying passive waveguide. In section C, the upper core is totally removed and only the passive waveguide is defined. The modes taking part in each section of the proposed structure are also shown in Fig. 1.

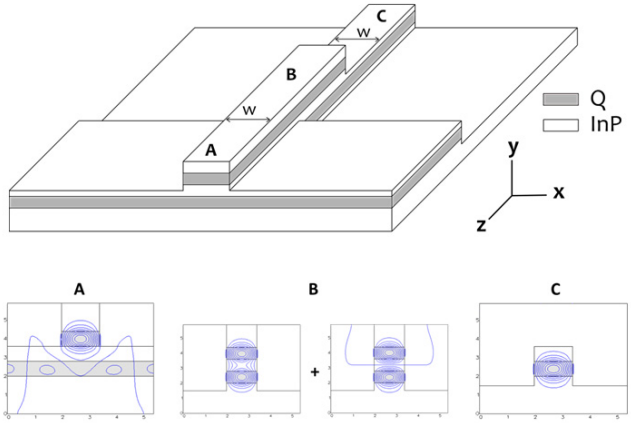

Fig. 1. Schematic drawing of the proposed new integration approach. The insets show the field distribution of the propagation modes in each section.

3. Design and simulation results

3.1 Waveguide design

The epitaxial layer structure is schematically shown in Fig. 2(a). This structure consists of a 0.8-μm-thick InGaAsP layer (with a bandgap cutoff wavelength of λ_g=1.13 μm, and a refractive index of 3.297), a 0.8-μm-thick InP separation layer, and an MQW active waveguide. The MQW region is composed of six 80-Å-thick 1% compressively strained InGaAsP (λ_g=1.55 μm) quantum wells separated by 150-Å-thick InGaAsP (λ_g=1.13 μm) barriers and sandwiched between two 190-nm-thick InGaAsP (λ_g=1.13 μm) separate confinement heterostructure layers. For this active region, an equivalent index of 3.297 with a thickness of 0.8 μm was computed.

#193754 - $15.00 USD Received 11 Jul 2013; revised 27 Aug 2013; accepted 27 Aug 2013; published 19 Sep 2013

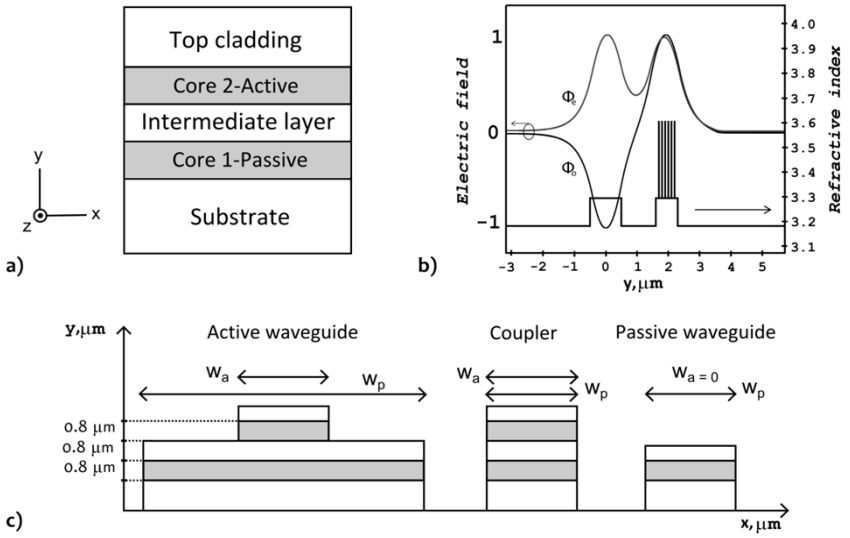

Fig. 2. (a) Layer structure of the vertically phase matched cores. (b) Refractive index and normalized mode profiles of the even and odd supermodes of the structure. Φe and Φo are respectively, the even and odd mode profiles of the structure. (c) Transverse structure of the waveguides in each region of the device.

The even (Φ_e) and odd (Φ_o) vertical supermodes are shown in Fig. 2(b). The vertical symmetry of the coupled waveguides is modified by the definition of laterally etched confinement walls over both cores leading to two concentric vertically stacked waveguides (see Fig. 2(c)). The relation between the widths of the upper active (w_a) and the lower passive (w_p) waveguides determines the modal behavior of the structure. In order to keep light in the active core, the upper core is etched leaving the underlying core unetched ($w_p = \infty$). The width of the active waveguide w_a has an important influence in the leaky loss of the amplified mode and will be discussed in detail in the next section. Equally etching both cores ($w_a = w_p$), a vertical resonant coupler is achieved in order to provide efficient power transfer between two waveguides. Totally removing the active core ($w_a = 0$) a monomodal structure is achieved whose fundamental mode propagates in the passive waveguide.

As shown, the transverse structure of each region is formed by two coupled waveguides. The two supermodes in each region can be expressed as a column vector with two components, each of one being the amplitude of the fundamental mode of each isolated waveguide [15,16].

$$\Phi_e(z) = \frac{1}{\sqrt{2}}\begin{vmatrix}\left(1-\frac{\delta}{S}\right)^{\frac{1}{2}}\\ \left(1+\frac{\delta}{S}\right)^{\frac{1}{2}}\end{vmatrix} e^{-i\beta_e z}, \quad \Phi_o(z) = \frac{1}{\sqrt{2}}\begin{vmatrix}-\left(1+\frac{\delta}{S}\right)^{\frac{1}{2}}\\ +\left(1-\frac{\delta}{S}\right)^{\frac{1}{2}}\end{vmatrix} e^{-i\beta_o z} \tag{1}$$

Equation (1) shows the expressions of both supermodes, where $\delta = (\beta_2-\beta_1)/2$ is the mismatch of propagation constants between the individual uncoupled waveguide modes, $2S = 2(\delta^2 + k^2) = \beta_e-\beta$ is the difference between the propagation constants between of the supermodes, and k is the coupling factor between the two waveguides. If the individual waveguides are phase matched ($\delta = 0$) the supermodes present perfectly symmetric and antisymmetric field distributions. If the two individual waveguides are phase mismatched ($k/\delta \to 0$), the supermodes approach to the modes in uncoupled single-waveguides modes.

#193754 - $15.00 USD Received 11 Jul 2013; revised 27 Aug 2013; accepted 27 Aug 2013; published 19 Sep 2013

3.2 Active waveguide optimization

Figure 3(a) shows the transverse structure of the active section or region A. The field distributions of the supermodes supported by the structure are also shown (see Figs. 3(b) and 3(c)). The width difference between the active (w_a = 1.4 μm) and the passive waveguides breaks the phase matching condition of the vertical layers and therefore, the even supermode is nearly an unpractical slab mode, and the odd supermode is strongly confined in the active waveguide. The confinement factor of this mode in the QWs is similar to that of the individual active waveguide and it will be favoured in the amplification, discriminating the fundamental order mode of the coupled system. This fact makes this approach much more flexible than the ATG structure, where the confinement factor decreases due to the proximity of the underlying passive core and has to be designed as a compromise with taper length [12]. Another feature of this structure is the fact that light travels on the waveguide having the lower effective index.

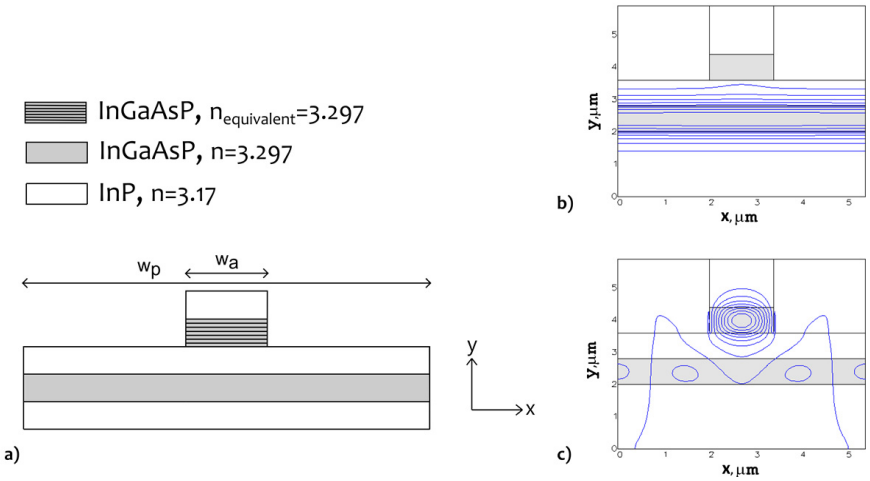

Fig. 3. (a) Schematic representation of the coupled waveguides system in the active region A, formed by a rib waveguide over a slab one. (b) Modal field distribution of the fundamental eigenmode of the structure. (c) Modal field distribution of the first order eigenmode of the structure.

Due to the tail in the optical power distribution of the first order mode (see Fig. 3(c)) in the infinite slab core, a constant optical radiation is produced laterally, meaning that such mode is a leaky mode [17]. The leaky loss reaches values of the order of tenths of dB/cm, depending of the width of the waveguide. Although such high losses can be compensated by the gain in the active layers, they can cause undesired effects in laser performance.

In order to reduce the leaky losses, a bending radius is applied to the active waveguide looking for antiresonance conditions for the multiple reflections that the leaky field undergoes in each of the two interfaces of the passive core (see Fig. 4(a)).

A commercial three-dimensional complex mode solver (Fimmwave) is used to calculate the bending loss of the active waveguide structure for different curvature radii. The fully vectorial mode solver is based on the film mode matching method [18] which, in case of curved waveguides, solves the Maxwell equations in cylindrical coordinates. Transparent boundary condition [19] is used in both sides of the simulation window to absorb the power leaked out of the bend and through the underlying slab waveguide, avoiding any parasitic reflection. Since no radiation is produced towards the other two transverse directions of the considered structure, a perfect magnetic conductor is used as boundary condition for the top and the bottom of the simulation window (see Fig. 4(b)). With this scheme the mode solver allows the calculation of the losses and propagation constants of the different modes.

#193754 - $15.00 USD Received 11 Jul 2013; revised 27 Aug 2013; accepted 27 Aug 2013; published 19 Sep 2013

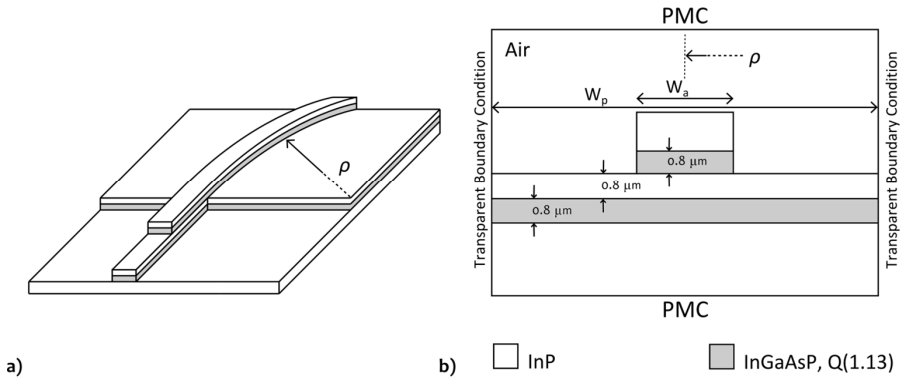

Fig. 4. (a) Three dimensional representation of the proposed integration approach with a passive waveguide, a resonant coupler and a bent active waveguide. ρ represents the bending radius of the active waveguide. (b) Cross-section of the simulated structure and detail of the boundaries used in the simulation: PMC stands for perfect magnetic conductor.

Figure 5 shows the total radiation loss (bending and leaky) for five different rib widths (w = 1.2, 1.4, 1.7, 2 and 2.5 μm) and for bend radii ranging from 1000 μm to 20 μm for TE polarization. Each graph presents two different regimes. A constant reduction of bending loss with decreasing radius is observed for sufficiently large values of the bending radius. For a range of smaller values, the bending loss oscillates with decreasing radius. This behavior is totally different from bend losses in standard waveguides, where they increase exponentially when bending radius decreases. In order to confirm these results, all the simulations have been performed using FDTD, whose results perfectly match those shown in Fig. 5.

The oscillations in the low range of values for the radius present deep and sharp minima, reaching lower bend loss than 0.1 dB/90° for several combinations of bend radius and waveguide width. A safe working point from the fabrication point of view is a width of 2.5 μm and a radius of 610 μm, providing a loss lower than 0.01 dB/90° which equals a linear loss of 0.1 dB/cm. For this working point there is no need to incorporate a physical offset between sections A and B (see Fig. 1) in order to improve the coupling efficiency at the interface. Moreover, the reflection expected in such interface is in the order of −70 dB, appropriate for the operation of active devices such as lasers.

Results in Fig. 5 also show other minima over a wide range of the radius: from around 800 μm to several tenths of micrometers, which allows for the design of devices requiring sharper bends such as ring and microring lasers. This fact can be considered as a novel advantage of the proposed approach compared to ATG technology, where the proximity of the passive core leads to huge bending losses for the fundamental mode of the structure.

Taking into account the position of the minima as a function of the waveguide width, we see a clear displacement towards higher bending radii for wider ribs. We can consider that the optimum design of the active waveguide in the lower leaky loss working point, can be controlled by these two parameters: the radius and width of the waveguide, which are defined during the lithography of the devices.

#193754 - $15.00 USD Received 11 Jul 2013; revised 27 Aug 2013; accepted 27 Aug 2013; published 19 Sep 2013

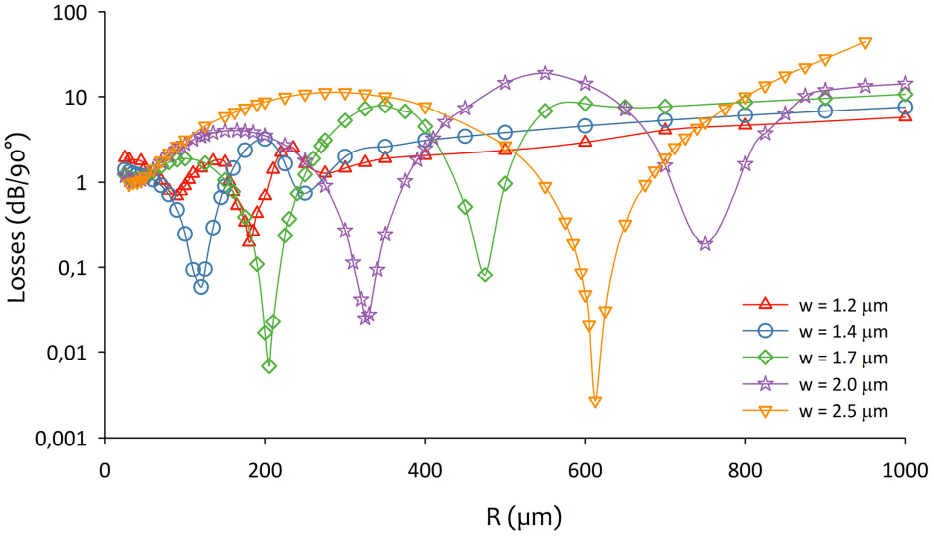

Fig. 5. Calculated loss for the first order supermode of the structure as a function of bend radius for different rib widths and TE polarization.

The oscillatory behavior for bending losses can be understood as the interaction under weak coupling conditions between a guided mode (the mode in the upper rib waveguide) and a set of lossy modes (the set of modes of the lower slab waveguide). The coupling of light from the guided mode in the upper rib waveguide to the underlying slab waveguide depends upon the effective index of the light propagated in the rib waveguide. This effective index is dependent on the bend radius of the waveguide, and as a consequence, coupling of light between both waveguides is maximized for certain curvature radii and minimized for others. As a consequence the imaginary part of the propagation constant for the first order eigenmode of the structure exhibits an oscillatory dependence on the bending radius. A similar performance was reported in 1986 for optical fibers with a protective coating with higher refractive index than the cladding [18].

Figure 6 shows the evolution of the imaginary part of the effective index of the first order supermode of the active structure as a function of the bending radius and the width of the waveguide.

#193754 - $15.00 USD Received 11 Jul 2013; revised 27 Aug 2013; accepted 27 Aug 2013; published 19 Sep 2013

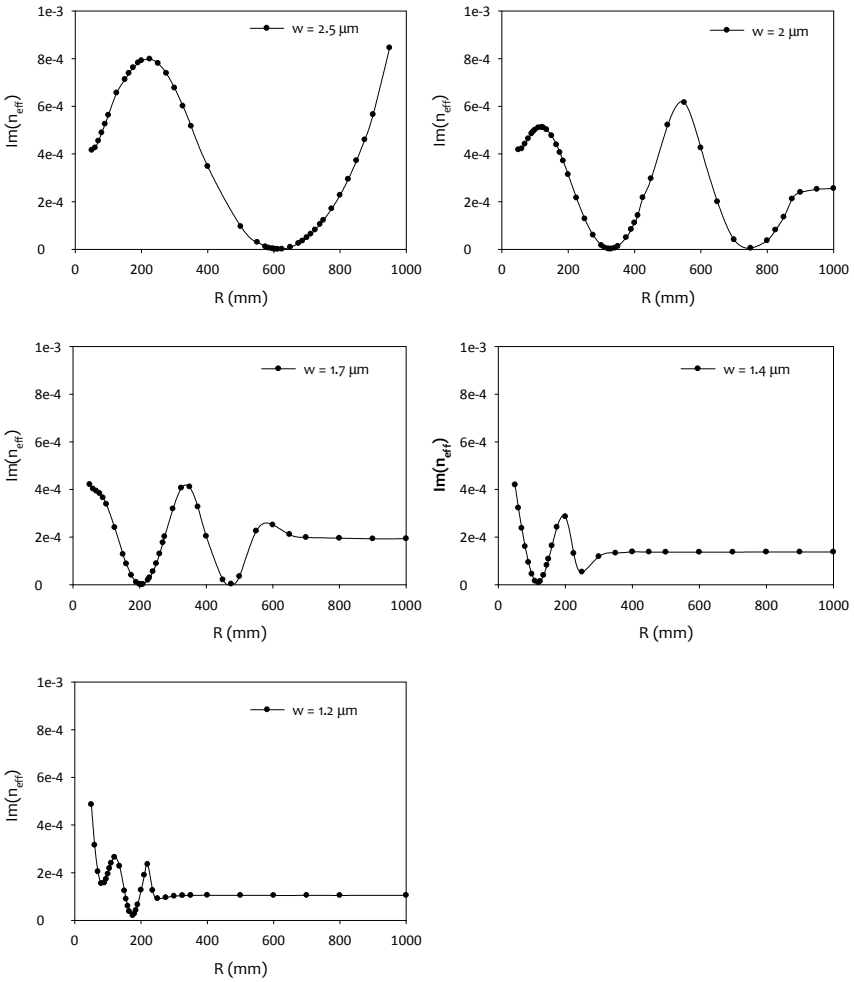

Fig. 6. Imaginary part of the effective index as a function of the bending radius and rib width (TE polarization).

The narrow minima in Fig. 5 and their displacement of several hundreds of micrometers for a variation of 1.3 µm in the width of the waveguide, predict a strong influence of this parameter during the fabrication process, hence a small tolerance to deviations from the nominal value. We have performed a set of simulations (see Fig. 7) to investigate the influence of changes in the width of the active waveguide around the minimum loss points, which are listed in Table 1.

Table 1. Minimum leaky and bending loss radius for each rib width

w (µm)	R (µm)
1.2	180
1.4	120
1.7	205
2	325
2.5	610

As predicted the structure is rather sensitive to width deviations: variations of at most ± 50 nm are needed to keep losses beneath 0.3 dB/90° in every designed point.

#193754 - $15.00 USD Received 11 Jul 2013; revised 27 Aug 2013; accepted 27 Aug 2013; published 19 Sep 2013

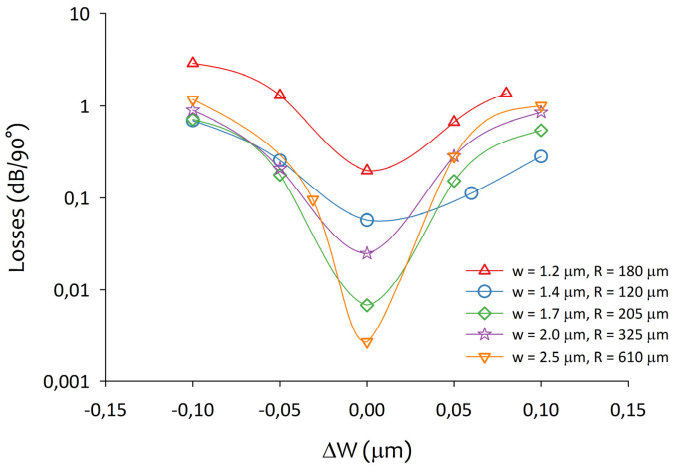

Fig. 7. Total propagation loss (bend and leaky) as a function rib width variations for the optimum loss working points shown in Table 1 (TE polarization).

It is important to notice that with a tolerance of ± 150 nm in the active section rib, losses are still kept below 2.5 dB/90°. This value may be problematic for the performance of passive devices albeit it is still good enough for active devices featuring typical material gain values. In addition, the process affected by the active rib width tolerance is not an alignment, but a hard mask definition and etching process, for which these values are not a big challenge [20,21].

3.3 Resonant coupler

The optical mode generated in the upper active waveguide reaches the vertical coupler identified as region B in Fig. 1. Since the core layers are vertically phase matched and the width of both waveguides is the same, the optical power is periodically transferred between the waveguides due to the mode beating of the even and the odd supermodes of the structure. Figure 8 shows the coupling efficiency of the vertical coupler in region B as a function of the coupling length and for the previously considered five different rib widths.

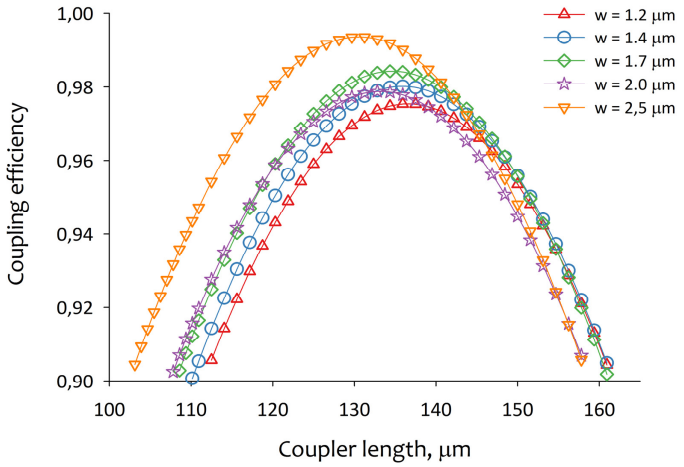

Fig. 8. Coupling efficiency between the upper and lower core (TE polarization).

Very efficient power transfer, higher than 97% (less than 0.15 dB losses), is obtained for every different width. The beating length shifts slightly from 136 μm for a width of 1.2 μm to 123 μm for the wider waveguide (2.5 μm). Therefore, a much higher fabrication tolerance is

#193754 - $15.00 USD Received 11 Jul 2013; revised 27 Aug 2013; accepted 27 Aug 2013; published 19 Sep 2013

expected for this parameter, when compared to the active section rib width. A new set of simulations has been performed to investigate the influence of changes in the width of the coupler Δw and in the refractive index contrast Δn. Figure 9 plots the efficiency of the five optimal coupler lengths (each coupler length optimized for its corresponding target waveguide width) as a function of changes in the width of the coupler waveguides. Results show a very relaxed behavior of this section as a function of width deviations during fabrication.

At this point we notice that the beat length is around a factor of 4 shorter than in the adiabatic approach, which would need several hundreds of micrometers (higher than 500 μm using the same active layer structure) to achieve such high power transfer and reasonable tolerances to width variations [14]. Furthermore, the proposed approach avoids submicron photolithographic features, which are needed in adiabatic tapers in order to obtain a complete mode displacement to the passive core.

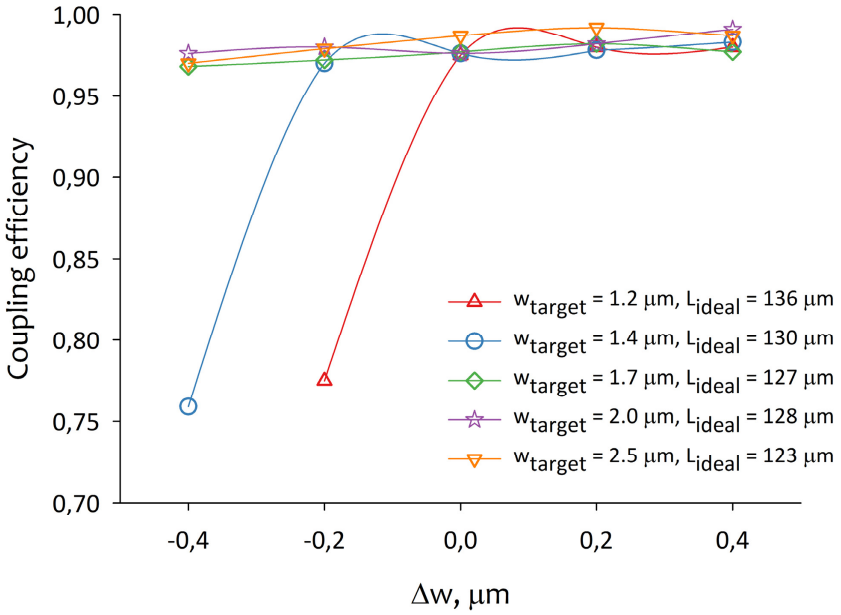

Fig. 9. Coupler efficiency as a function of width variations for each target waveguide width and its corresponding optimal coupler length. (TE polarization).

Figure 10 shows the influence of variations in the waveguide refractive index during the growing process of the wafer. We have made the assumption that the variation in the refractive index alters both waveguides in the same way. The resonant coupler performance drops less than a 10% from its optimal value for deviations of ± 0.5% in the waveguides refractive index. This deviation supposes a difference of ± 14% taking into account the difference between the core and the cladding refractive indices (Δn). Again, a larger fabrication tolerance is expected for these two parameters (width of the coupler and refractive index contrast).

#193754 - $15.00 USD Received 11 Jul 2013; revised 27 Aug 2013; accepted 27 Aug 2013; published 19 Sep 2013

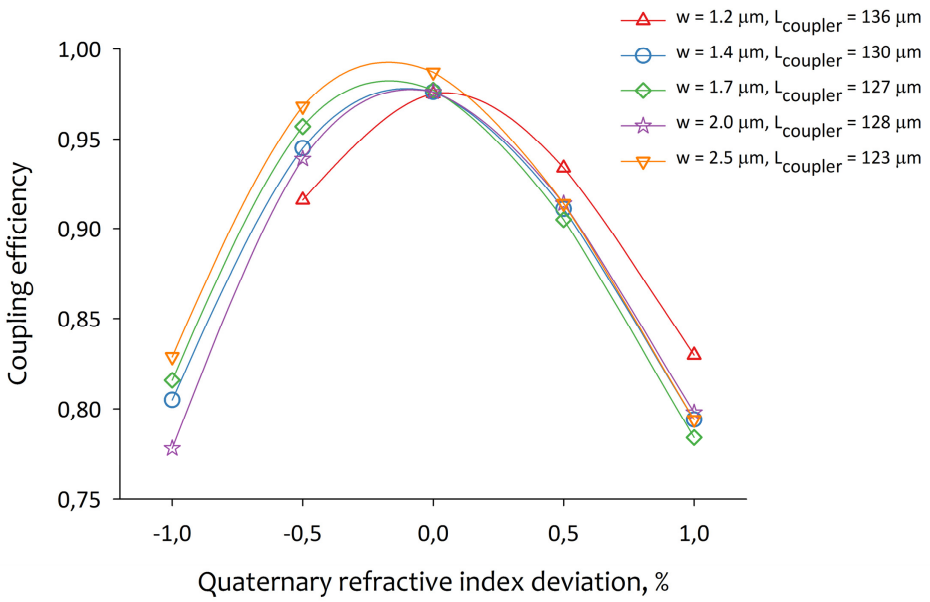

Fig. 10. Coupling efficiency as a function of waveguide refractive index variations. The target quaternary refractive index is 3.297 (TE polarization).

4. Conclusions

In this work, we have presented a new active-passive integration approach for photonic components using a vertical stack of two coupled waveguides. This technology is based on the control of the asymmetry of the coupled system by means of the ratio between the widths of the upper and lower waveguides. A structure with a rib waveguide over a slab one is proposed in order to maintain the light in the upper waveguide. This structure presents an oscillatory dependence of the bend loss as a function of the bend curvature. Minimum loss points exhibiting less than 0.1 dB/90° have been found through simulation. The power transfer between the upper active waveguide and the underlying passive waveguide is obtained for equal width in both waveguides. Efficiencies higher than 97% (less than 0.15 dB of losses) have been achieved for coupler lengths shorter than 130 µm. Tolerances as low as ± 50 nm in the active section rib width are the main technical drawback for this structure. The coupling section presents however a much lower sensitivity to variations in the width and the refractive index during device fabrication.

The proposed approach shows several advantages compared to the ATG technology with adiabatic tapers: 1) the confinement factor of the amplified mode in the QWs does not depend on the design and proximity of the passive core, 2) the minimum bend loss points of the active waveguide allow for the design of new devices such as ring and microring lasers, 3) the power transfer length of the coupler is around a factor of 4 shorter than the adiabatic design, and 5) it avoids submicron photolithographic features.

Acknowledgments

This work was supported by the Spanish Government project TEC2010-20224-C02-01.

#193754 - $15.00 USD Received 11 Jul 2013; revised 27 Aug 2013; accepted 27 Aug 2013; published 19 Sep 2013